Numerical Simulation of Weak Force Measurements

Antoni Bandachowicz

University of Chicago

May, 2023

Contents

1 Introduction

1.1 The Weak Force and Nuclear Spin-Dependent Parity Violation (NSD-PV)

The weak nuclear force constitutes one of the four fundamental forces in nature and is responsible for a range of processes, from beta decay to neutrino interactions and nuclear fusion[1]. Recent research efforts focus on measuring the strength of the weak force's parity-violating (PV) components. Parity (one of the three discrete space-time symmetries) describes the behavior of physical laws under spatial inversion [2]. As has been demonstrated by Wu et al, interactions between particles governed by the weak force violate parity symmetry [3], meaning they favor one parity state over another. The ZOMBIES experiment aims to measure the strength of the parity-violating component of the weak force caused by nuclear spin within atoms. Nuclear spin-dependent parity violation (NSD-PV) primarily arises from Z^0 boson exchange between electrons and the nucleus, as well as from the interaction between electrons and the parity-violating nuclear anapole moment [2][4].

The aim of this thesis is to numerically simulate the mixing of opposite parity states of Barium monoFluoride (BaF) within the ZOMBIES experiment, which is directly caused by NSD-PV. During preparation and initial testing of the ZOMBIES experiment, several sources of systematic error have been identified. Thus, this thesis also aims to numerically reproduce the behavior of the systematic error present when a non-reversing unipolar electric field is present alongside depletion laser detuning within gap 22 of the ZOMBIES experiment. The physics behind the mixing of parity states of BaF are explained in section 1.2. The setup of the ZOMBIES experiment is detailed in section 2, and the precise behavior of the systematic error being simulated is described in section 3.

1.2 Barium monoFluoride (BaF) and Parity States

The ZOMBIES experiment measures the NSD-PV in $^{138}Ba^{19}F$, a molecule chosen for its enhancement effect of NSD-PV caused by its rotational structure. $^{138}Ba^{19}F$ has unpaired electron spin, which means it systematically has small energy splitting between opposite-parity hyperfine states, which can be mixed by NSD-PV, allowing the PV signal to be measured. The ground electronic state of $^{138}Ba^{19}F$ is described by the Hamiltonian

$$H = B_e N^2 + \gamma \mathbf{N} \cdot \mathbf{S} + b\mathbf{I} \cdot \mathbf{S} + c(\mathbf{I} \cdot \mathbf{n})(\mathbf{S} \cdot \mathbf{n}).[2] \quad (1)$$

The opposite parity states of the molecule are written in terms of the decoupled basis $|N, m_N\rangle$ $|S, m_S\rangle$ $|I, m_I\rangle$ where $\mathbf{N}$ is rotational angular momentum, $\mathbf{S}$ is electron spin, γ is the spin-rotation constant, b and c are hyperfine constants, $\mathbf{I}$ is spin of the molecule, and $\mathbf{n}$ is the unit vector along the internuclear axis. It is the mixing between two of these states of opposite parity that allows us to measure NSD-PV effects. The two ground states that the ZOMBIES experiment mixes are $X^2\Sigma(v = 0, N^P = 0^+, J = 1/2)$, $X^2\Sigma(v = 0, N^P = 1^-, J = 3/2)$. The exact treatment of these ground states and Hamiltonian is described in Emine Altuntas' thesis [5].

1.3 The 2D Effective Hamiltonian and the Asymmetry

The effective Hamiltonian describing the mixing of the two opposite parity states can be expressed within the Hilbert space composed of the two states. This leads to a 2-dimensional matrix of the form

$$\hat{H} = \begin{bmatrix} 0 & iW + d \cdot \epsilon(t) \\ -iW + d \cdot \epsilon(t) & \Delta \end{bmatrix} \tag{2}$$

where W is the weak force matrix element, $d = -3360 \times 2\pi\text{Hzm/V}$ is the electric dipole moment of the BaF, $\epsilon(t)$ is the electric field that the BaF is subject to, and Δ is the B-field detuning that brings the opposite parity states to near degeneracy. The value of the weak force component is extracted in the following way. We input $\hat{H}$ and the wavefunction of BaF $|\Psi(t)\rangle$ into the time-dependent schrödinger equation, $i\hbar\frac{\partial}{\partial t}|\Psi(t)\rangle = \hat{H}|\Psi(t)\rangle$, which gives us two differential equations that we can solve to find the solutions to the probability amplitudes $C_+(t)$, $C_-(t)$. From these equations, we can solve for the populations of each state and the signal S where $S \propto |C_+|^2$. This gives us a solution for the signal of the form

$$S = 4\left(\frac{d\epsilon\omega}{\omega^2 - \Delta^2}\right)\left[\frac{d\epsilon\omega}{\omega^2 - \Delta^2}\sin^2\left(\frac{\Delta T_e}{2}\right) + 2\frac{W}{\Delta}\sin^2\left(\frac{\Delta T_e}{2}\right)\sin^2\left(\frac{\Delta T}{2}\right)\cos\left(\frac{\Delta}{2}(T_{f1} - T_{f2})\right)\right]$$

Using the solution for the signal we can express an analytical solution for the asymmetry signal of the form

$$A(\Delta) = \frac{S(+\epsilon_0) - S(-\epsilon_0)}{S(+\epsilon_0) + S(-\epsilon_0)} \tag{3}$$

which explicitly gives

$$A_{sim}(\Delta) = 2\frac{W}{\Delta}\frac{\omega^2 - \Delta^2}{d \cdot \epsilon_0 \omega}\frac{\sin[\Delta/2 * T_{max}]}{\sin[\Delta/2 * T_e]}\cos[\frac{\Delta}{2}(T_{f1} - T_{f2})] \tag{4}$$

Where T_{f1} is the time the BaF beam travels undisturbed from the first depletion laser to the ϵ-field, T_{f2} is the time it takes for the BaF to travel from the ϵ-field to the second depletion laser, and T_e is the time the BaF beam spends within the ϵ-field. These are all values dictated by the setup of the ZOMBIES experiment, which is detailed in section 2.

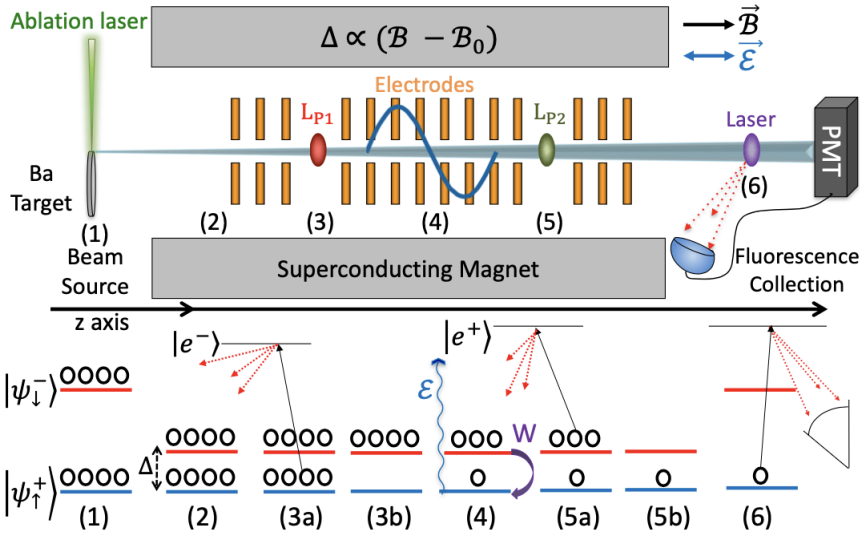

Figure 1: Schematic of the apparatus (top) and the evolution of parity level populations (bottom) [6].

2 Experimental Setup

To understand the entire process of systematic error simulation, we must look into the procedure of the ZOMBIES experiment. We use a pulsed, supersonic molecular beam of BaF, produced via ablating Ba metal with a pulsed laser in the presence of fluorine gas, SF6 (region 1 in figure 1). Rapid expansion carries the gas into vacuum, cooling the beam to 30K. Next, the molecules in the beam move into a large solenoid magnet, which brings the even and odd parity levels to near crossing via Zeeman shifts (region 2 in figure 1). At this step, both parity levels are equally populated due to the finite temperature of the beam. Then, we apply an 860 nm diode laser to the beam, which is tuned to deplete (empty) the detection state (even parity state) via optical pumping. Molecules are pumped to a level that has a low probability of decaying back into the detection state (region 3 in figure 1). Following the laser, the beam travels into an oscillating electric field, which is applied over a distance L_e. The electric field has form $\varepsilon = \varepsilon_o sin(2\pi * z/L_e)$. Note that the electric field is parallel to the magnetic field in this region. Although the field is static in time, it changes based on position (it is position dependent). This means the molecules in the beam experience a time-dependent electric field. A single sine cycle induces a Stark transition of molecules from the odd parity state to the previously emptied even parity state (region 4 in figure 1). The interference between the electromagnetic field and the weak force results in a term that is proportional to ϵ_o, meaning that this interaction creates the term in the signal that allows us to determine the parity asymmetry. After the electric field, the non-detection level (odd parity state) is depleted using optical pumping (region 5 in figure 1). After the second laser, the molecules exit the magnet, and we detect the number of

molecules in the even parity state via laser-induced fluorescence with a PMT. Using an 860nm laser, we excite the molecules in the even parity state to a higher energy level. Molecules in this excited state are further excited by a second laser, which excites them to an even higher energy level. We observe the decay fluorescence from this higher level. Repeating this whole procedure with a reversed electric field ($-\varepsilon_o$) provides the parity violation asymmetry.

2.1 Gap 22 and The ε_{nr} Pulse

The IR is composed of 28 consecutive, circular rings encapsulating the BaF beam. This isolates the beam from the outside environment. Ring 22 is a prism ring, which directs the second depletion laser into the IR, allowing it to interact with the BaF beam. Gap 22 is the separation between ring 22 and ring 23. The simulation of the experiment will focus on interactions occurring at this gap between the depletion laser and an amplified unipolar ϵ_{nr} pulse. ϵ_{nr} fields are stray, non-reversing electric fields. By non-reversing, we mean fields that do not change when we reverse the voltages used to generate the field. Unipolar ϵ-field pulses have a nonzero pulse area (meaning the integral of the electric field strength with respect to time in a given point of space is non-zero). It has been discovered in previous experiments that the coupling of non-reversing ϵ-fields with detuning from resonance δ of the second depletion laser caused a significant shift in the weak force matrix element W. In order to test the behavior of this shift in W, an amplified non-reversing field is simulated at gap 22. The simulated unipolar pulse has form:

$$\varepsilon^u_{nr} = \varepsilon^u_{nr0} sech(\frac{z - z_0}{\sigma_u}) \tag{5}$$

where z_0 is the center location of gap 22, and for a 1 V voltage step. The resultant field has a varied amplitude ϵ^u_{nr0} and $\sigma_u = 0.76$ cm. Here $z = vt$, where $v = 616$ m/s is the molecular beam speed. The total simulated electric field becomes:

$$\varepsilon(t) = \varepsilon^u_{nr0} sech(\frac{2\pi * v}{\sigma_u}[t - t_{L2}]) + \varepsilon_0 sin(\frac{2\pi * vt}{L_e}). \tag{6}$$

Here, $t_{L2} = 103.7\mu$ s is the time at which the BaF hits the second depletion laser, and $L_e =$ 0.0538m (t=0 at the first depletion laser) is the length over which the reversing ϵ-field term is active.

2.2 The Second Depletion Laser and Laser Detuning

The current ZOMBIES experiment contains four external cavity diode lasers (ECDL) to address the transitions for state preparation and eventual detection. The second depletion laser is a home-built ECDL which drives the transition that depletes the non-detection odd parity state

onto the higher energy excited state. More explicitly, the second depletion laser drives the $X^2\Sigma(v = 0, N^P = 1^-) \rightarrow A^2\Pi_{1/2}(J^P = 5/2^+)$ transition. We simulate the effect of this depletion laser on the state of the BaF molecules by writing the resulting Rabi frequency as a Gaussian centered at $t = t_{L2}$,

$$\Omega(t) = \Omega_0 * \exp\left\{\frac{-(t - t_{L2})^2}{2\sigma^2}\right\} \tag{7}$$

Where $\Omega_0 = \gamma = 2\pi \times 0.3$ MHz and $\sigma = 1.6 \times 10^{-6}$ s. This form is obtained by the fact that the laser varies in intensity as the BaF beam travels through it.

3 Systematic Error in the Weak Force Component

A systematic offset in the NSD-PV weak matrix element W was observed experimentally when an exaggerated ϵ_{nr} pulse was applied to gap 22. The effect was not consistently reproducible in size, which led Altuntas and researches of the ZOMBIES experiment to believe that the error was due to imperfections in the experimental system [5]. Since gap 22 is to the right of the second depletion laser, there could be a link between data taken with ϵ_{nr} pulse and imperfections with the second laser, notably the laser's detuning from resonance δ. As a result, a series of measurements were made while intentionally amplifying the unipolar ϵ_{nr} pulse centered at Gap 22. The following behaviors were noted about the offset in W:

1. Systematic offset in W has a linear dependence on the peak amplitude of the unipolar pulse centered at gap 22 (ε_{nr0}).
2. The slope of W/ε_{nr0} is roughly proportional to the detuning offset value, δ.
3. There is no effect on W when no unipolar pulse is present at gap 22.

As a result, we established that the equation for the weak force component offset was of the form

$$W = C_W * (\varepsilon_{nr0} * \delta)[5] \tag{8}$$

where $C_W = 0.09$ is a constant found experimentally. For typical values of δ and ϵ_{nr} within the experiment, $\epsilon_{nr} = 1.3 \pm 4.7$mV/cm and $\delta = 0.3 \pm 1.3$ MHz. This means that the expected offset under normal experimental conditions is $W_{error}/2\pi = 0.04 \pm 0.21$ Hz[5].

4 Procedure

In order to numerically simulate the systematic error, we need to describe the experimental system in a way that takes into account the high-energy excited state ($A^2\Pi_{1/2}(J^P = 5/2^+)$)

onto which the BaF molecules are optically pumped by the second depletion laser. We also need to introduce parameters that represent the possible imperfections of the laser (such as detuning from resonance and amplitude fluctuations). Because of spontaneous emission into the high energy excited state and considerations of laser imperfections, it becomes easier to treat the system using density matrices.

4.1 Re-Expressing the Effective Hamiltonian

We start by defining a new Hilbert space, now containing three dimensions representing the two parity states and the high energy excited state. These are the $X^2\Sigma(v=0, N^P=0^+, J=1/2)$, $X^2\Sigma(v=0, N^P=1^-, J=3/2)$, and $A^2\Pi_{1/2}(J^P=5/2^+)$ energy states of the BaF molecule, as described in the introduction section. Our operators are now expressed within our new 3D Hilbert space, which means $\hat{H}$ and $\hat{\rho}$ are now 3D matrices. Within $\hat{H}$, we added optical pumping terms expressed in terms of the Rabi frequency $\Omega(t)$. These come from the Rotating Wave Approximation (RWA), which allows us to simplify the interaction between the laser and BaF beam. $\Omega(t)$ is related to the resonant frequency of the system and the laser. Finally, we add an additional term δ representing the detuning of the 2nd depletion laser. Equation 9 shows the described 3D Hamiltonian. Δ represents the B-field detuning in the experiment, which causes a decrease in the energy difference between opposite parity states.

$$\hat{H} = \begin{bmatrix} 0 & iW + d*\epsilon(t) & \frac{\Omega(t)}{2} \\ -iW + d*\epsilon(t) & \Delta & 0 \\ \frac{\Omega(t)}{2} & 0 & \delta \end{bmatrix} \tag{9}$$

$$\hat{\rho} = \begin{bmatrix} \rho_{--} & \rho_{-+} & \rho_{-e} \\ \rho_{+-} & \rho_{++} & \rho_{+e} \\ \rho_{e-} & \rho_{e+} & \rho_{ee} \end{bmatrix} \tag{10}$$

Inputting $\hat{H}$ and $\hat{\rho}$ into the Von Neumann equation, $i\hbar\frac{\partial\hat{\rho}}{\partial t} = [\hat{H}, \hat{\rho}]$, we obtain nine optical Bloch equations (OBEs). The OBEs allow us to describe the time evolution of the populations of each state, as well as the time evolution of the coherences between each state. Displayed are the three OBEs which allow us to describe the evolution of the populations:

$$i\hbar\frac{\partial\rho_{--}}{\partial t} = [iW + d\cdot\epsilon(t)]\rho_{+-} + \Omega/2\rho_{e-} - [iW + d\cdot\epsilon(t)]\rho_{-+} - \Omega/2\rho_{-e} \tag{11}$$

$$i\hbar\frac{\partial\rho_{++}}{\partial t} = [-iW + d\cdot\epsilon(t)]\rho_{-+} - [iW + d\cdot\epsilon(t)]\rho_{+-} \tag{12}$$

$$i\hbar\frac{\partial\rho_{ee}}{\partial t} = \Omega/2\rho_{-e} - \Omega/2\rho_{e-} + i\hbar\gamma\rho_{ee} \tag{13}$$

We have manually added spontaneous emission terms with a decay rate "γ" to matrix elements related to the high energy excited state. These terms represent the rate at which molecules in the excited state decay into other states of lower energy outside of our Hilbert space. These spontaneous emission terms cause the populations to be non-normalized. We input the resulting 9 OBEs into Mathematica's *NDsolve* function to numerically solve this system of complex partial differential equations using finite difference methods. For the test cases, we analyse the behavior of the populations of each state against time. For the asymmetry values, we extract the value of the even parity population at time $t = t_{max} = 110\mu$s. We go into more detail about the simulated asymmetry values in section 5.3.

4.2 Simulating the Behavior of the Systematic Error Arising From Laser Detuning and Unipolar Pulse Presence

Once the behavior of our 3D Hamiltonian has been properly formulated by the OBEs, we moved on to simulating the behavior of the systematic error noticed by Altuntas when examining the interaction between the second depletion laser and the ϵ_{nr} pulse [5]. We turned the observations described in section 3 into test scenarios:

- **Scenario 1**: We should observe no effect on W when no unipolar pulse is present. We can simulate this case by setting $\epsilon_{nr0} = 0$ and $\delta = 2\pi * 0.3$MHz.
- **Scenario 2**: We expect a linear relationship between W and ϵ_{nr0}. To simulate this, we vary values of ϵ_{nr0} and plot the resulting change in W. We do this for four different values of δ, namely $\delta = 2\pi * [0.3, -1, 2.7, -2.7]$MHz.
- **Scenario 3**: We expect the slope of $\mathrm{W}/\epsilon^u_{nr0}$ to be roughly proportional to the detuning value δ. To show this, we plot the slopes of linear relationships from scenario 5 against their respective δ values.

In these scenarios, we numerically integrated the OBEs from the moment the first depletion laser hits and set this event as t=0. This means that the second depletion laser hits the beam at time $t = t_{L2}$. We also introduced the reversing field ϵ_r, which is a single sine cycle starting at $t = t_{e1} = 7.4\mu$s and ending at $t = t_{e1} = 94.8\mu$s. $\Omega(t)$ was re-expressed as a Gaussian with amplitude $\Omega_0 = \gamma$ and width $\sigma = 1.6 \times 10^{-6}$ s, as described in section 2.2.

4.3 Finding Asymmetry Values and Extracting W

In order to test the behavior of the systematic error described by the scenarios, we needed to extract the value of W. To do this, we found asymmetry values at time $t = t_{max} = 110 \times 10^{-6}$s while varying $\Delta/2\pi$. The simulated asymmetry points were found using equation 3, where, as

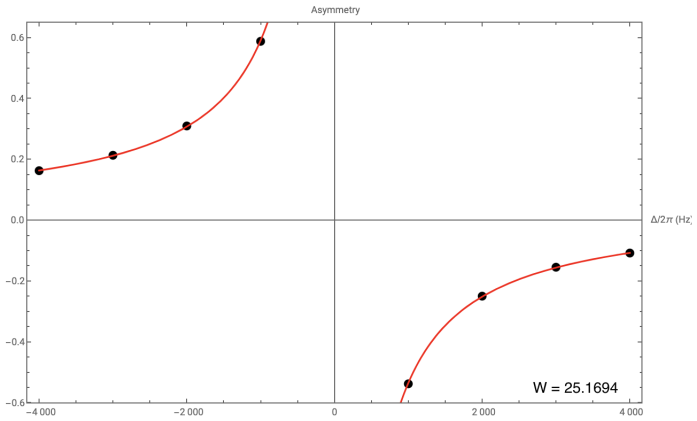

Figure 2: Asymmetry points against varied values of $\Delta/2\pi$. The red line represents the simulated fit described in equation 14. This example is for the case where $\delta = -2.7$ MHz and $\epsilon_{nro} = -12$ V/m.

before, the notation $S(+\epsilon_0)$ represents the value of the population of the even parity state at time $t = t_{max}$ when the reversing ϵ-field magnitude is positive. $S(-\epsilon_0)$ is the population when the ϵ-field magnitude is negative. In other words, $S(+\epsilon_0) = \rho_{++}(t = 110\mu\text{s})$. Once asymmetry values for different $\Delta/2\pi$ were found, the points were fitted to a modified analytical solution compared to the one described in the introduction. The fit function had form

$$A_{sim}(\Delta) = 2\frac{W}{\Delta}\frac{\omega^2 - \Delta^2}{d \cdot \epsilon_0 \omega}\frac{\sin[\Delta/2 * T_{max}]}{\sin[\Delta/2 * T_e]}\cos[\frac{\Delta}{2}(T_{f1} - T_{f2})] + a_1\Delta + a_0 \tag{14}$$

where $T_{f1} = 7.4\mu$s is the time the BaF beam travels undisturbed from the first depletion laser to the ϵ-field, $T_{f2} = 8.9\mu$s is the time it takes for the BaF to travel from the ϵ-field to the second depletion laser, and $T_e = 87.4\mu$s is the time the BaF beam spends within the ϵ-field. a_0 and a_1 are fit parameters.

5 Analysis

Scenario 2 and scenario 3 have been successfully simulated using the 3D Hamiltonian formulation. By looking at figure 3a, we see data following linear relationships of W against varying non-reversing ϵ-field amplitude, ϵ_{nr0}, with all fits having coefficients of determination $R^2 > 0.99$. We also see a negative linear relationship for negative values of δ, as has been observed experimentally [5]. Analyzing the behavior of a_0 and a_1 allows us to further infer on the accuracy of the simulation. From the experimental results described in chapter 7.5.2 of Altuntas' thesis [5], we expect a_0 to vary proportionately with the magnitude of ϵ_{nr}, which we can observe in figure 3 (b).

Figure 4 demonstrates the behavior of the slopes (W/ϵ_{nr0}) of fits in figure 3a for varying

$W_{input}/2\pi$ (Hz)	$W_{output}/2\pi$ (Hz) when $\Omega_0 = \gamma$	$W_{output}/2\pi$ (Hz) when $\Omega_0 = 0$
-5	19.9246	19.2989
0	23.8317	23.8317
5	27.3992	27.9668

Table 1: fitted W for varied W_{input}. These values are plotted in figure 5.

values of δ. This roughly confirms the behavior expected in scenario 3, with a coefficient of determination at $R^2 = 0.995$, though it is difficult to confirm the behavior exactly due to the limited range of points plotted. Additionally, we found a slope of 0.0455 for the fit in figure 4, suggesting that the change in W/ϵ_{nr0} is roughly proportional to half the change in detuning δ. This goes against what has been measured by Altuntas, with an experimental value of the slope at 0.09 ± 0.01 Hz, which puts the simulated value at $51 \pm 5\%$ of the experimental value.

It is worth noting that all of the extracted values for W were found to have a shifted value of $W_{shift}/2\pi = 23.8317$Hz. Subsequently, the values of all of the points shown in figure 3 have been adjusted to this shift. The shift also occurs for the case where $\epsilon_{nr0} = 0$ and $\delta = 2\pi * 0.3$MHz, suggesting a failure to correctly simulate scenario 1. Further analysis goes into possible sources of this shift in extracted values of W.

5.1 Analysing the Failure to Reproduce Scenario 1

In order to find the source of the shift in W values ($W_{shift}/2\pi = 23.8317$ Hz) we analyzed the reaction of the system to changes in different input parameters. Since the shift was present when no ϵ_{nr} peak was present, it was assumed that our term for laser detuning δ could have caused the shift. Additionally, the effect of the Rabi frequency of the laser $\Omega(t)$ was put into question since we did not know how the values of the peak and the width of the Gaussian describing $\Omega(t)$ in equation 7 affected the W measurement. Moreover, we wanted to gauge the ability of our model to provide an extracted W value if we inputted a nonzero value for W in our 3D Hamiltonian, which we called W_{input}.

As a result, we analyzed the behavior of W when $\Omega_0 = 0$ and $\Omega_0 = 0.3 * 2\pi$ MHz, while also varying W_{input}. The results are shown in figure 5, as well as in table 1. We notice that the shift is still present despite the lack of influence from the depletion laser or the unipolar pulse. We can also see that our model roughly outputs the correct W value if we account for W_{shift}. Currently, we are uncertain about the source of W_{shift}. However, we managed to rule out $\Omega(t)$, δ, and ϵ_{nr} as probable sources.

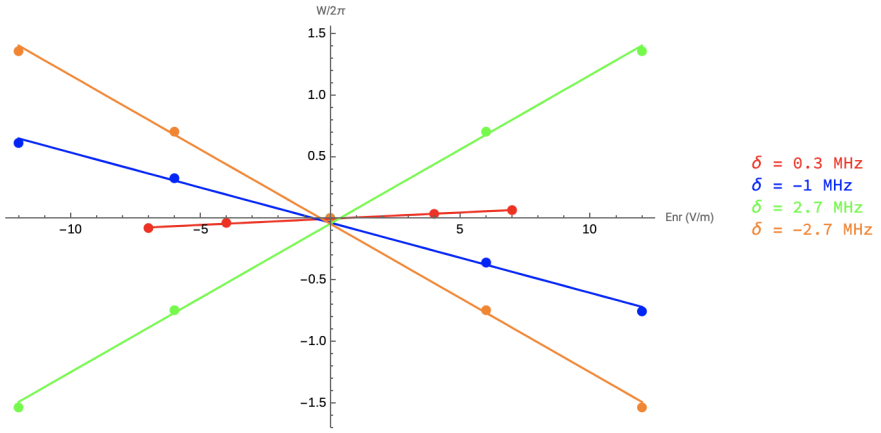

(a) Linear fits of W/2π against ϵ_{nr0} for varying values of δ.

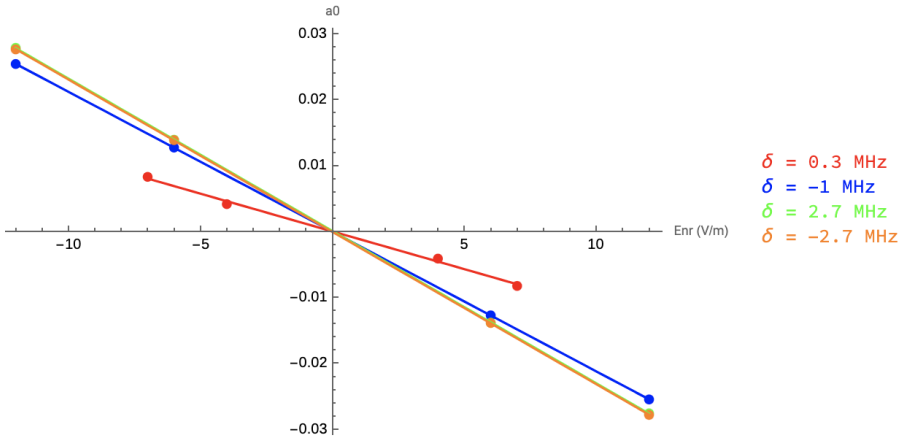

(b) Linear fits of the fitting parameter a_0 against ϵ_{nr0}.

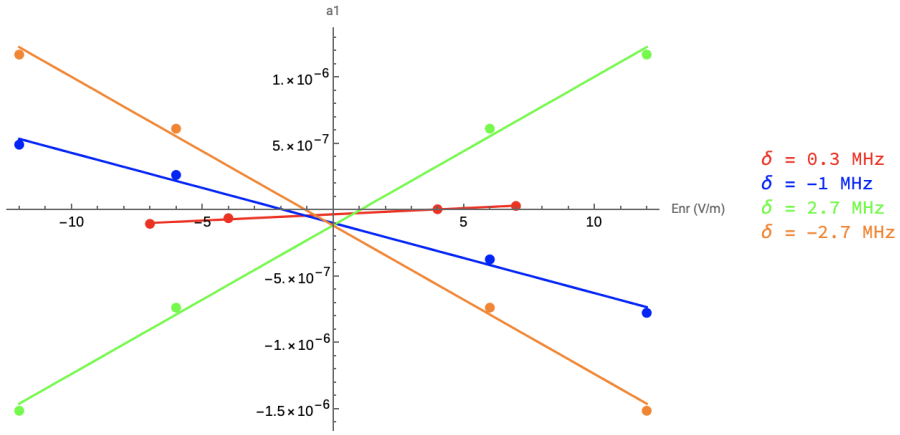

(c) Linear fits of the fitting parameter a_1 against ϵ_{nr0}.

Figure 3: Analysing the relationship between W and ϵ_{nr0}. Figure (a) demonstrates linear relationships for varying values of laser detuning δ. The relationship becomes negative for negative values of δ, which accurately reproduces the behavior of the systematic error found experimentally.

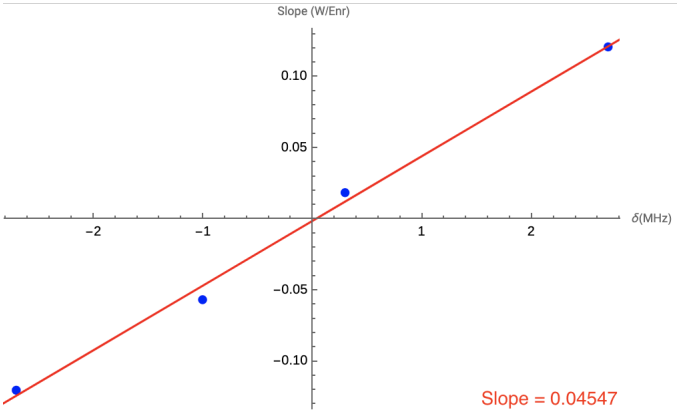

Figure 4: Slopes (W/ϵ_{nr}) of fits from figure 3 against laser detuning δ. The extracted slope of this linear relationship is 0.0455.

6 Conclusion

Out of the three behaviors of the systematic error described by our scenarios, only two have been simulated with some success. Most notably, we obtain a positive linear relationship between the slopes W/ϵ_{nr} of figure 3a and δ, suggesting a proportional increase in W with increasing magnitude of the combination of ϵ_{nr} and δ. The simulation suffers from an unknown shift in the weak force matrix element W equivalent to $W_{shift}/2\pi = 23.8317$ Hz. After analysing potential contribution from δ and $\Omega(t)$ terms within the simulation, the source of the shift is yet to be determined.

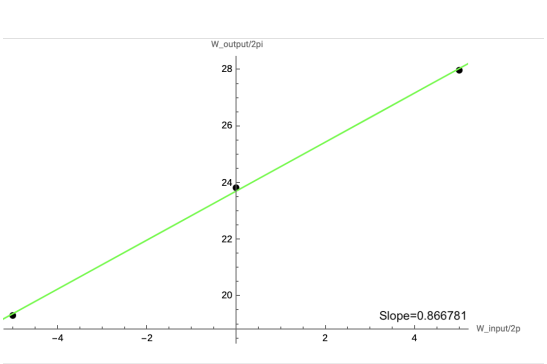

(a) Behavior of fitted W against inputted W with no depletion laser present ($\Omega(t) = 0$)

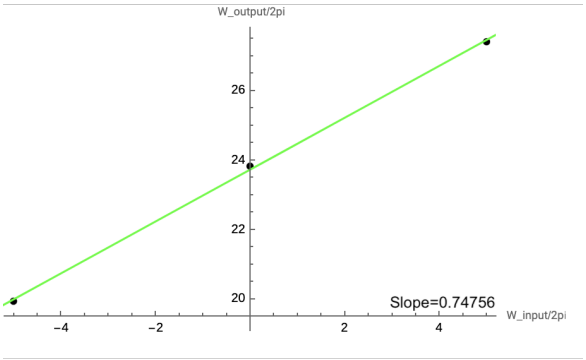

(b) Behavior of fitted W against inputted W with depletion laser present ($\Omega(t) = 0.3$ MHz)

Figure 5: Analysing the behavior of W_{shift} for input values of $W_{input}/2\pi = -5, 0, 5$ Hz. Both subfigures show simulations for the case where $\delta = 0$. The shift is still clearly present, suggesting that the shift is not caused by δ. The fits also suggest that the model could be accurate in modeling the behavior of systematic error if we account for W_{shift}.

References

[1] Brian Robson. Weak nuclear force. *Modern Physics Letters A*, 36:2130009, 02 2021.

[2] Emine Altuntas, Jeffrey Ammon, Sidney B. Cahn, and David DeMille. Demonstration of a sensitive method to measure nuclear-spin-dependent parity violation. *Physical Review Letters*, 120(14), apr 2018.

[3] C. S. Wu, E. Ambler, R. W. Hayward, D. D. Hoppes, and R. P. Hudson. Experimental test of parity conservation in beta decay. *Phys. Rev.*, 105:1413–1415, Feb 1957.

[4] Jens Erler and Shufang Su. The weak neutral current. *Progress in Particle and Nuclear Physics*, 71:119–149, 2013. Fundamental Symmetries in the Era of the LHC.

[5] Emine Altuntas. *Measurement of Nuclear Spin Dependent Parity Violation in 138Ba19F*. PhD thesis, Yale University, 2017.

[6] Emine Altuntaş , Jeffrey Ammon, Sidney B. Cahn, and David DeMille. Measuring nuclear-spin-dependent parity violation with molecules: Experimental methods and analysis of systematic errors. *Physical Review A*, 97(4), apr 2018.